The reproduction process of Gram-positive protocells

Dheeraj Kanaparthi[1,2&3*], Marko Lampe[4], Jan-Hagen Krohn[1&3], Falk Hildebrand[5], Thomas Boesen[6], Andreas Klingl[7], Prasad Phapale[8], & Tillmann Lueders[2&3]

Affiliations:

[1]Department of Cellular and Molecular Biophysics, Max-Planck Institute for Biochemistry, Munich, Germany.

[2]Chair of Ecological Microbiology, BayCeer, University of Bayreuth, Germany.

[3]Excellenzcluster ORIGINS, Garching, Germany.

[4]Advanced Light Microscopy Facility, European Molecular Biology Laboratory, Heidelberg, Germany.

[5]Quadrum institute, Norwich, UK.

[6]Department of Biosciences, Center for Electromicrobiology, Aarhus, Denmark.

[7]Department of Biology, LMU, Planegg-Martinsried, Germany.

[8]European Molecular Biology Laboratory, Heidelberg, Germany.

* Corresponding author

Abstract: Protocells are, by definition, the most primitive predecessors of biological cells, devoid of all complex molecular biological processes. They are believed to have mediated reproduction entirely by physicochemical forces. Despite these propositions, little is known about the actual mechanisms. To understand the reproductive process of protocells in their native habitat, here we used a top-down approach to transform bacterial cells into a primitive lipid vesicle like state in which cells are devoid of molecular biological mechanisms regulating their reproduction. Given protocells existed on early Earth, we conducted all our experiments under the presumed environmental conditions of Archaean Eon Earth. Even in the absence of functioning biological processes, cells under these conditions reproduced in a defined sequence of steps, always leading to the formation of viable daughter cells. Their reproduction mechanism can be explained by the interaction between intracellular metabolism, physicochemical properties of cell constituents, and environmental conditions. Based on our observations, we propose that reproduction may be an inherent property of cells with an internal metabolism without the need for dedicated molecular biological processes.

Introduction

The theory of chemical evolution proposes that prokaryotes evolved from more primitive protocells [1]. These cells are hypothesized to have been primitive and devoid of all complex molecular biological processes i.e., complex functional elements like proteins. This means that, processes like reproduction must have been entirely mediated by simple biophysical processes [2] under favorable environmental conditions. Our current understanding of protocells is primarily a result of studying lipid vesicles (LVs) with aqueous core as model protocells [2–4]. Despite accomplishing considerable progress in our understanding of protocells, we believe LVs do not represent protocells' true physiological or compositional complexity.

To replicate the complexity of a protocell, here we worked with protoplasts of Gram-positive bacteria as model protocells (*Exiguobacterium strain M* protoplasts –*EM-P*). Our choice of using bacterial protoplasts is based on three key considerations. First, protocells like bacterial protoplasts were most likely devoid of a peptidoglycan cell wall. Synthesis of individual cell wall components, transporting them across the cell membrane, and assembling them into a cell wall is a physiologically complex process require a multitude of enzymes, working in a coordinated manner[5,6]. Evolutionarily primitive protocells most certainly are considered to have been devoid of such complex intracellular processes. Second, like the protocells, protoplasts lack an innate ability to regulate their morphology or mediate reproduction[7–9]. They can be described as a sack of cytoplasm reproducing in a haphazard manner[10]. The same should have been true for the protocells, at least upto a certain stage of evolution. Third, even the most primitive cell must possess three essential characteristics – a mechanism of harvesting free energy from the surrounding, a mechanism of using this energy to sustain minimal biosynthetic processes, replication, and transfer of its genetic material it to the daughter cells. Possessing even these fundamental processes incorporates considerable cytoplasmic complexity. Hence, we believe that the protocell cytoplasm most likely resembled bacterial cytoplasm, not in its molecular biological complexity but in its biophysical properties. Given these similarities between protocells and protoplasts, we argue that bacterial protoplasts could be a better proxy for studying protocell reproduction than LVs.

Self-assemble of lipids into LVs, happens within a narrow pH range and is influenced by environmental conditions like temperature and salt content[11]. Hence, most protocell studies are conducted under well-controlled laboratory conditions. These experimental conditions

rarely resemble the environmental conditions of early Earth. Studying an organism outside its natural habitat provides an incomplete understanding of its ecological function and behavior. This is especially true for protocells, given their greater dependence on environmental conditions to mediate essential cellular functions like reproduction. Hence, we believe any attempt to understand their reproduction should be conducted in their natural habitat. To achieve this objective, we grew *EM-P* under the environmental conditions mimicking those that could have been prevalent on early Earth. Recent geological studies suggest that Earth's surface had cooled enough to accommodate liquid water during the Hadean Eon[12], creating ecological conditions conducive to the emergence of life[13]. The earliest unambiguous evidence of life exhibiting complex CO_2 fixation pathways dates to 3.8 billion years ago (early Archaean Eon)[14,15]. This means that first appearance of primitive protocells, most likely happened during the late Hadean or early Archaean Eon[16]. The exact environmental conditions of Archaean Earth are currently unclear. Nevertheless, an emerging consensus among the scientific community suggests that at least by 3.8 billion years ago, surface temperatures likely ranged between 26° and 35°C[17,18]. Early Earth's oceans are also hypothesized to be 1.5 to 2 times saltier than the present-day oceans[19]. To replicate these conditions, we grew *EM-P* in half-strength tryptic soy broth amended with 5-8% (w/v) Dead Sea Salt (TSB-DSS) at 30°C. We used DSS, rather than pure NaCl, in our experiments better to simulate the complex salt compositions of natural environments. We then monitored these cells at regular intervals using super-resolution microscopy to understand if and how these cells grow and reproduce. In the following sections of the manuscript, we present the lifecycle of *EM-P* under Archaean Eon environmental conditions, followed by a mechanistic explanation.

Results

Physiological characterization of protoplasts

Exiguobacterium strain M (*EM*) was transformed into protoplasts, as described in the methods section. This transformation of "wild-type" *Exiguobacterium strain M* (*EM*) into its protoplast state (*EM-P*) was evident from the change in morphology from bacillus to spherical morphology. Besides morphology, considerable differences were observed in the physiological behavior of *EM* and *EM-P*. One such difference was the glucose metabolism under aerobic conditions (Figure S1). We observed the accumulation of fermentation products like lactate, acetate, formate, and ethanol when *EM-P* was grown in well-aerated media containing glucose as a sole carbon source. In contrast, no such formation of volatile fatty acids was observed in *EM* incubations. *EM* and *EM-P* also exhibited differences in catalase activity. *EM* exhibited an expected trend in catalase activity. Catalase activity was observed when the *EM* cells were grown under aerobic conditions (58.7 ± 6.2 U/ml), while little to no catalase activity was exhibited by *EM* under fermentation conditions (3 ± 0.8 U/ml). In contrast, *EM-P* showed catalase activity independent of the growth conditions. A similar level of catalase activity was observed when the cells were grown under aerobic (77.8 ± 5.3 U/ml) and anaerobic (65.3 ± 7.2 U/ml) conditions.

Reproduced either by budding or by binary fission

During the lag and early-log growth phase, *EM-P* gradually grew by an order of magnitude in diameter (Figure 1A, B & Video 1). Subsequently, the spherical cells transformed into ovoid shapes (Figure 1C & Video 2). They then developed surface invaginations (Figure 1C, D & Video 2), which gradually got deeper, transforming an oval-shaped cell into two distinct

daughter cells (Figure 1D & Video 3). These cells subsequently underwent fission, resulting in individual daughter cells. We occasionally saw cells undergoing fission but connected by a thin membrane tether (Video 3). Despite having the appearance of binary fission, no uniformity was observed in the sizes of the daughter cells (Figure 1D-I). Depending on the size of the daughter cells, cells in this growth stage appear to be reproducing either by budding (Figure 1F-I) or by binary fission (Figure 1C&D, & Video 1-3).

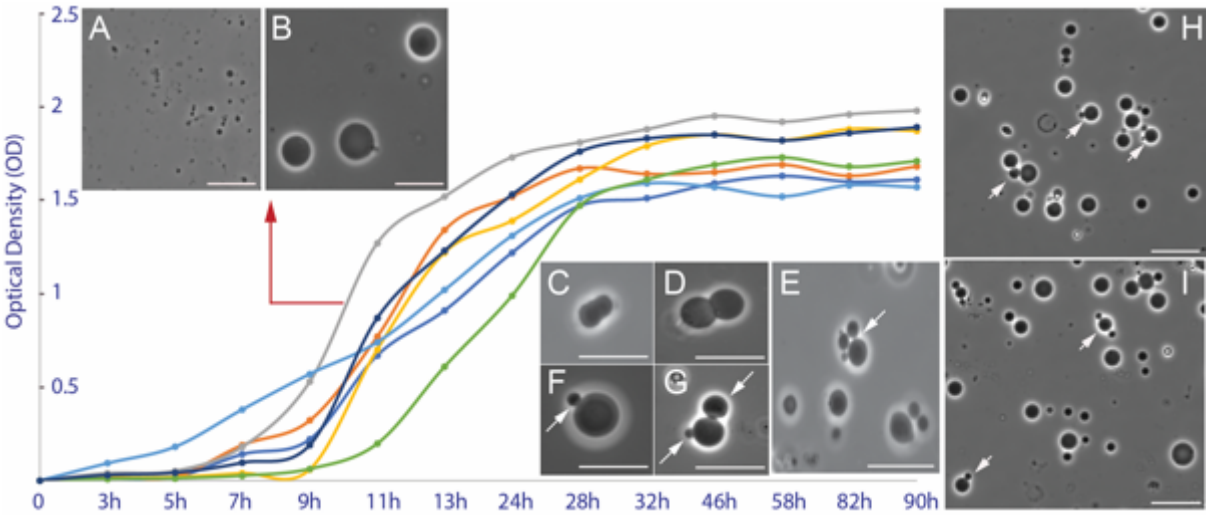

Figure 1. Growth characteristics of *EM-P* in batch culture. *EM-P* exhibited a typical sigmoid growth curve with an initial phase of slow growth rate (lag phase), a log phase with exponentially increasing cell numbers and a gradual decline in the growth rate during the stationary phase. The X and Y-axis in the plot indicate the time in hours (h) and optical density. Images A & B shows typical morphologies of cells in early and late lag-phase (notice an increase in the size of the cells). Images C - I, show early log phase cells that seems to be reproducing either by binary fission (C, D and Video 2 & 3) or budding (arrows). Images F – I show variation in the sizes of the daughter cells (buds). Scale bars: 10µm.

Most cells in this growth stage were in a constant state of surface undulations (Video 1-3). Treatment of cells with bactericidal compounds like 0.5% glutaraldehyde and formaldehyde, although killed the cells, which is evident from the lack of growth when sub-cultured into new media but did not result in a static cell state. The surface undulations were only observed to be halted when the cells were treated with detergents like 0.5% Triton X100.

In the subsequent growth stages, *EM-P* was observed to be reproducing by two different processes. In brief, *EM-P* either reproduced by the forming external or internal daughter cells. Sequential steps involved in reproduction by the formation of external and internal daughter cells are shown in Videos 4-11 and Videos 12-18, respectively.

Reproduction by forming external daughter cells

The formation of external membrane extensions during the late log phase happened in a series of steps (Figure 2). Cells first formed hollow bud-like structures from multiple locations on the cell surface (Figure 2C&D). In the subsequent growth stages, these buds transformed into short filamentous extensions, often covering the entire surface of the cell (Figure 2E, 3C&D & Video 5). Some cells had filamentous tentacles encompassing the entire cell surface (Video 5). These filamentous extensions were in a constant state of movement and never static.

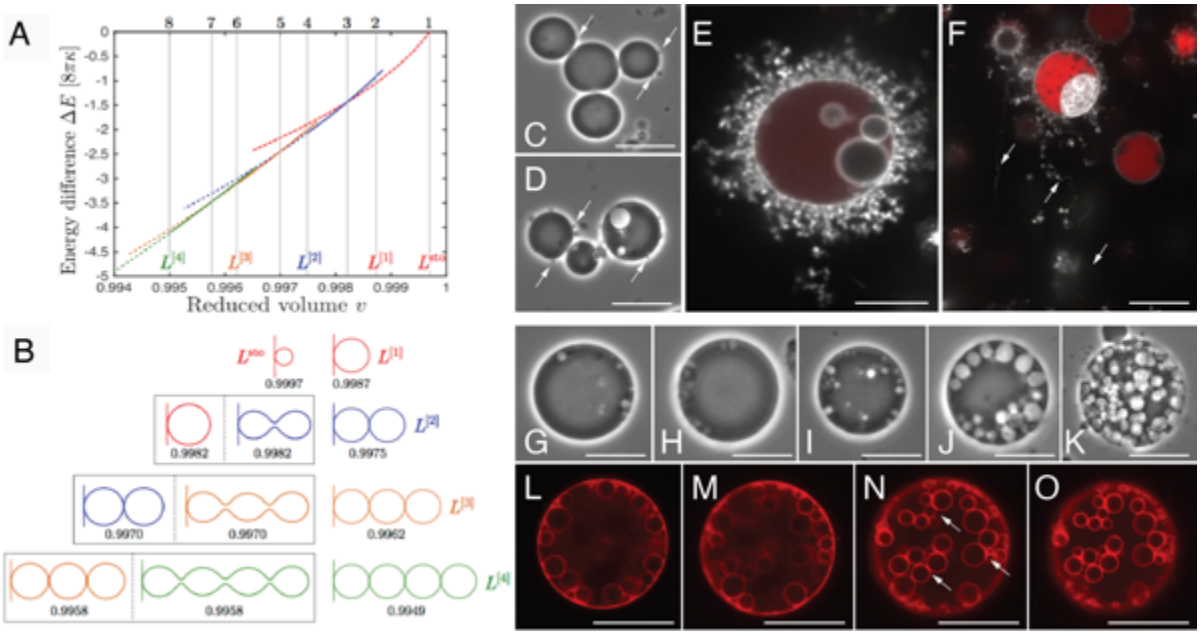

Figure 2. Comparison between theoretically predicted steps in filament formation to observation in *EM-P*. Images A & B were originally published by Liu *et al.,* 2015[20]. Image A shows energy landscape of different equilibrium shapes as a function of reduced volume (v). ΔE indicates deflation induced reduction in bending energy. Image B shows the shapes of filamentous extensions corresponding to eight vertical lines in image A. Images C-O show images of *EM-P* cells from different growth stages with external (C-F) or internal membrane (G-O) structures that were formed in a pattern similar to what was theoretically predicted (A & B). Arrows in images C & D points to late-log phase *EM-P* cells with tiny membrane extensions. Image E show cells surface covered with short filamentous extensions. Image F show cells stationary growth stage cells with longer filamentous extensions. Cells in these images were stained with universal membrane stain, FM™5-95 (white) and DNA stain, PicoGreen™ (red). Images G-K show sequential stages observed in the development of intracellular vesicles. L-O show optical sections of a Nile red stained *EM-P* cell at different planes. Arrows in these images points to the interconnected nature of these vesicles, similar to $L^{(3)}$ and $L^{(4)}$ in image B. Scale bars: 10μm.

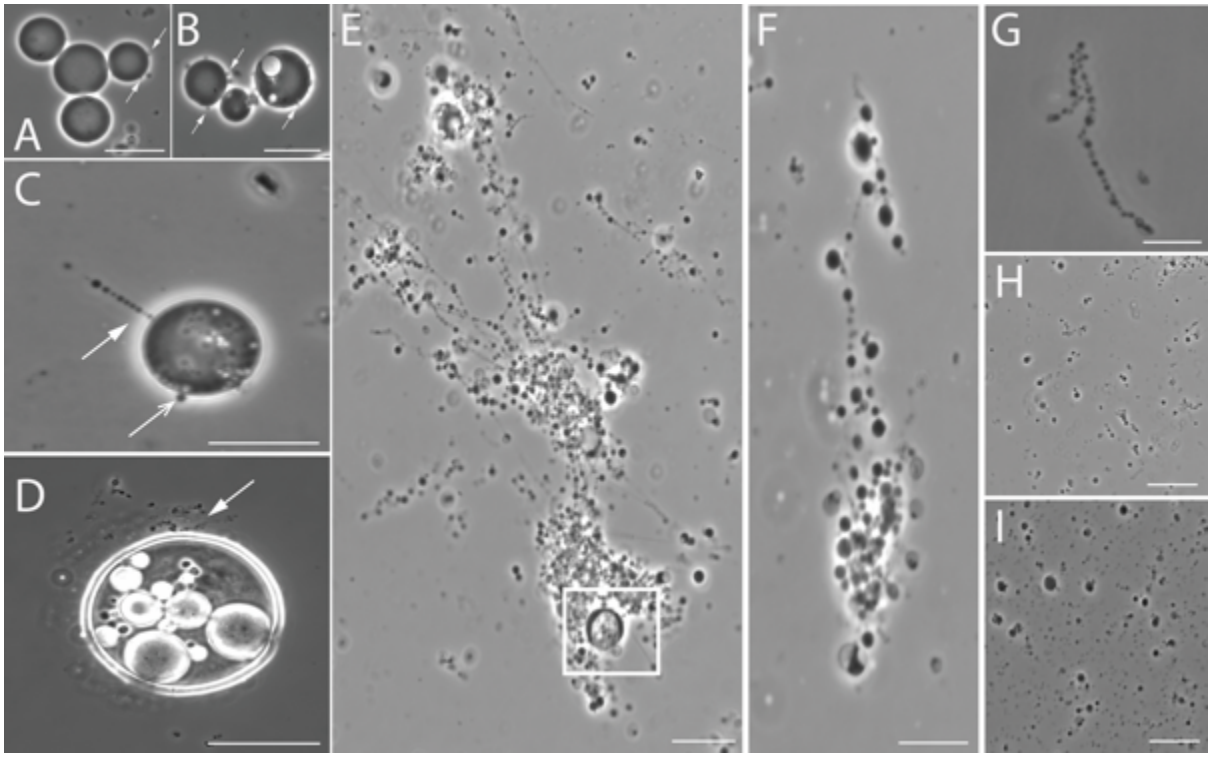

Figure 3. Life cycle of *EM-P* reproducing via formation of extracellular daughter cells. Image A&B show a late log phase cell with bud like structures on *EM-P* cell surface. Image C show a late log phase cell with open arrow pointing to surface buds and a closed arrow pointing towards filamentous extensions (also see Video 4). Image D shows a cell from a subsequent growth stage cells with multiple filamentous extensions (also see Video 5). Images E-F show formation of daughter cells as string-of-beads attached to a parent *EM-P* cell (boxed region) (also see Video 6-8). Images F-I show the detachment of these strings of daughter cells and their subsequent fragmentation into individual daughter cells (also see Video 9-11). Scale bars: 10μm (A-G).

Over time, the cytoplasm was transferred from the parent cell into these filaments (Figure 3C & Video 5-7). These filamentous extensions then developed surface depressions along their length resembling tubular vesicles subjected to curvature-induced destabilization at their surface (like Rayleigh-Plateau instability) (Video 6). This led to the transformation of the

filaments from a tubular into a “string-of-beads” morphology (Figure 3C-E & Videos 6-8). These strings of daughter cells are then detached from the parent cell and fragmented into individual daughter cells in a sequence of steps, as shown in Figure 3F-I (Video 8-11).

Reproduction by internal daughter cells

The first step in reproduction via intracellular daughter cells was the formation of intracellular vesicles (Figure 2G & 4A, white arrows). The sequential stages involved in the formation of these buds followed a pattern similar to that of the formation of filamentous extensions. During the late log phase intracellular vesicles were observed to have been relatively small and originated from multiple points on the cell surface (Figure 2G-I). Subsequently, these vesicles then grew in size, and dethatched from the cell membrane or transformed into a string of intracellular vesicles (Figure 2L-O and S2E & F, indicated by arrows in both the images). Sizes and numbers of these intracellular vesicles were heterogenous without a discernible trend, despite numerous repetitions (Figure S3).

Daughter cells were formed into the vesicles by a process similar to external daughter cells, via budding (Figure 4D, arrow). These buds were formed by the membrane undergoing positive membrane curvature, into the vesicle (Figure 4D). Such buds were formed from different points within a single vesicle (Video 13). These buds either dethatched from the vesicle surface and released into the vesicle as individual daughter cell (Figure 4F&H & Video 14) or grew into a string of daughter cells (Figure 4E & Video 14) and then fragmented into multiple daughter cells (Figure 4H). Note the cell on the left side of

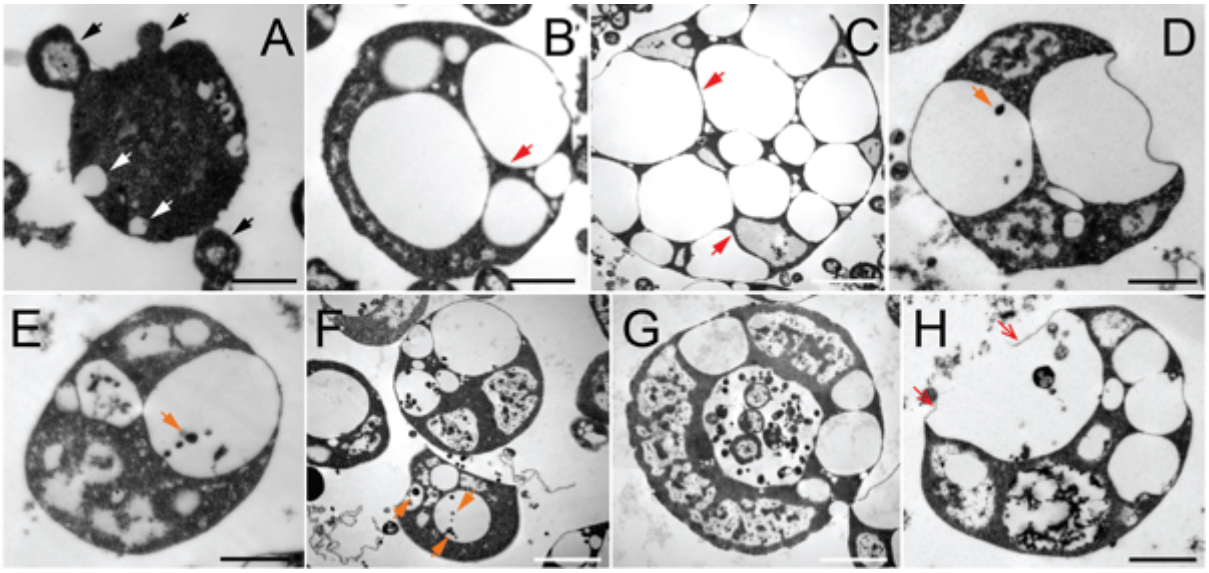

Figure 4. The life cycle of *EM-P* reproducing via the formation of intracellular daughter cells. Images A-H are TEM images of the life cycle of *EM-P* reproducing by the formation of intracellular daughter cells. Image A show the process by which intracellular (white arrows) vesicles and bud-like structures are formed (black arrows). Closed red arrows in images B & C point to the narrow cytoplasmic region of the cell. Arrows in images D-F points to the formation of individual and string of daughter cells or string of multiple daughter cells. Image G shows internal daughter cells with intracellular vesicles. Image H shows the process of daughter cell release by rupture of vesicle membrane (open red arrows). Scale bars: 1µm.

the video 14, which shows both individual and string-of-daughter cells. Daughter cells formed by this process were highly mobile (Video 14). Due to the gradual transfer of cytoplasm from parent to daughter cells (Figure 4D, E & S4), cytoplasmic content of the *EM-P* parent cells gradually got depleted (Figure S6). During the late stationary growth phase, many *EM-P* cells were hollow with intracellular vesicles (Figure 4G & S4) containing highly motile daughter cells (Video 14). Daughter cells were released into the surrounding media by

rupture of the cell or vesicle membrane (Figure 4H & Video 15-18). The final growth stage of *EM-P* was characterized by the presence of cells with all the above-described morphologies, along with a considerable amount of membrane debris (Figure S5).

Membrane phase separation in *EM-P*

To investigate the role of membrane phase separation, we stained our cells to differentially label different membrane phases. FM5-95™ stains the membrane irrespective of phase, while FAST-DiI™ partitions into the liquid-disordered (L_d) phase. We saw differential staining in all growth phases (Figure 5). In early growth stages, L_d-specific labeling showed small (< 180 nm) patches in the cell membrane, indicating formation of small L_d domains in a predominantly liquid-ordered (L_o) membrane (Figure 5A-C). The number of these L_d patches increased towards later growth stages. Eventually, membrane budding occurred in domains of both membrane phases, but in opposite directions: L_d membrane preferred to bud inward into the cytoplasm (Figure 4), whereas the L_o membrane budded outward (Figure 5).

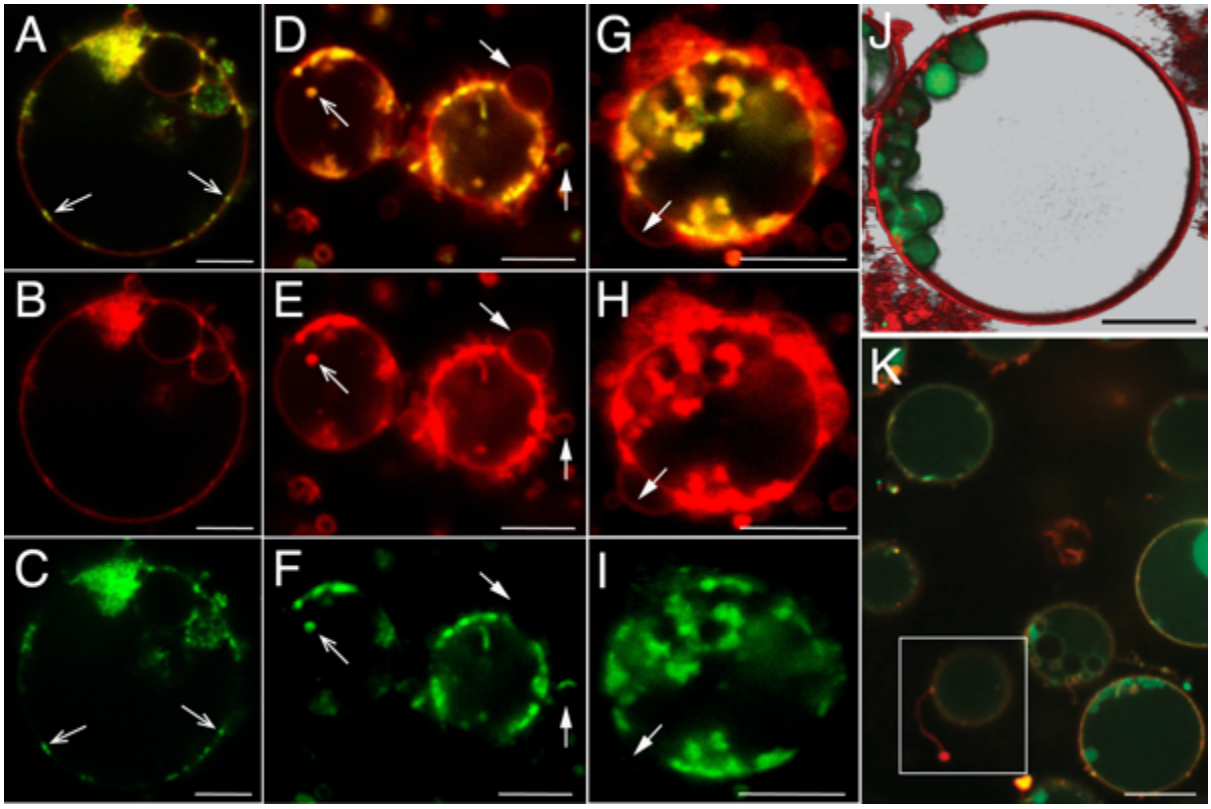

Figure 5. Membrane phase-separation in *EM-P*. Cells in these images were stained with FM™5-95 (all membrane, red) and *FAST*™ DiI (L_d-membrane, green) and imaged either using a super-resolution STED microscope (A-J), or a spinning disk confocal (K). Images A-C, D-F, and G-I are images of same cells in different confocal channels. Open arrow in A-F, point to small patches of L_d-membrane (≈ 180nm) (A-C) on the cell surface. Closed arrows in D-I: L_o-membrane extensions out of the cell. Images J is 3D-rendered image of intracellular vesicles composed of L_d-membrane within the cell. A series of optical sections of the stacks shown in Figure S6. Image K shows *EM-P* cells with filamentous extensions like shown in Figure 3C, entirely composed of L_o membrane (also shown in Video 19). Scale bars: 10µm (A-I) & 5µm (J & K).

Influence of environmental conditions on *EM-P*'s life cycle

Environmental conditions strongly influenced the morphology and reproduction process of *EM-P*. Cells grown in 7% DSS-TSB and 7% KCl-TSB were comparable in size and morphology. In comparison, cells grown in $MgCl_2$ (Figure 6) were significantly smaller in size than those grown in equivalent concentrations of DSS or KCl (Figure S7). Apart from the differences in the sizes, a more significant portion of cells grown in KCl developed intracellular vesicles with fewer external filaments (Figure S7). The diameter of most cells grown in $MgCl_2$ is restricted to 0.5-2μm and these cells reproduced mainly by forming extracellular daughter cells (Figure 6C-F). Also, in contrast to the above-described reproductive process, daughter cells formed by this process did not detach from the parent cell immediately. Over time, they formed an entangled web of daughter cells (Figure 6F). *EM-P* morphology also changed reversibly when cells were transferred between media containing different salt compositions.

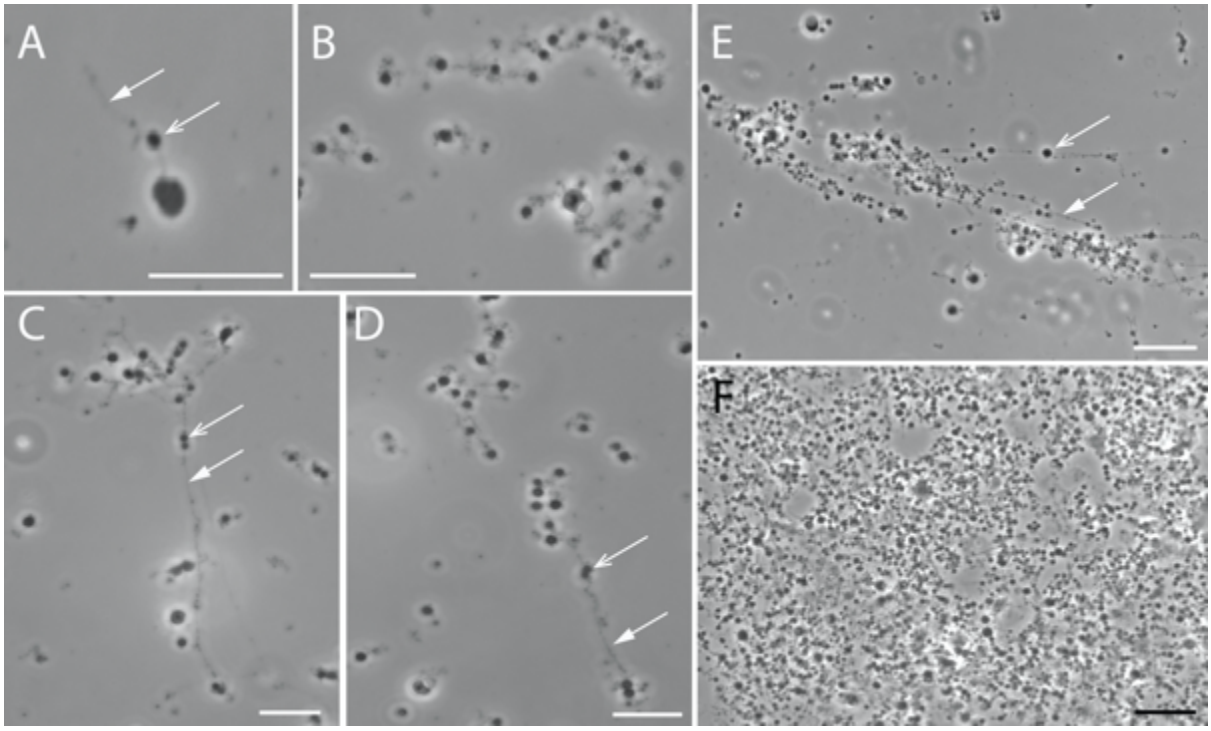

Figure 6. *EM-P* cells reproducing via external daughter cells in TSB-5%$MgCl_2$

Images A-F show sequential morphological transformation of *EM-P* when grown in the presence of 5% $MgCl_2$-TSB. Closed arrows points to membrane tethers connecting individual daughter cells. Open arrows in these images point to spherical daughter cells within the filaments. Image F show stationary growth phase cells. Cells during all growth stages are in a constant state of motion. To see these cells in motion please watch Videos 20 & 21. Scale bars: 10μm.

When grown on an orbital shaker, *EM-P* reproduced exclusively by binary fission. None of the above-described morphologies, like large cells with intracellular vesicles, strings of daughter cells, or membrane debris, was observed. Most cells observed under this type of growth resemble in size and shape the ones shown in Figure 1A-K. Transfer of the incubation bottles from an orbital shaker to a static incubator half-way through the experiment resulted in cells developing external filamentous extensions and intracellular vesicles in media containing DSS or KCl and filamentous extensions in media containing $MgCl_2$. These results suggest cells rapidly adapt their morphology to the incubation conditions.

Reproductive efficiency and viability of *EM-P* daughter cells

The loss of intracellular DNA during cell division was used as a proxy to determine the reproductive efficiency of *EM-P* (Figure 7). The intracellular and extracellular DNA concentrations during all growth stages are shown in Figure S8. Given the nature of *EM-P* reproduction (lysis and release of intracellular daughter cells – Figure 4H & Video 16), we expected some loss of intracellular constituents. However, we also observed spontaneous lysis of cells during all growth stages that is not associated with the release of daughter cells (Video 24&25). To understand if the lysis of cells was photo-induced during the imaging

process (by confocal or a STED microscope), we incubated cells under anaerobic conditions in the dark and imaged them only using more-gentle phase-contrast microscopy at fewer intervals (48h – 72h). No significant differences were observed in the amount of extracellular DNA concentrations between these incubations (Figure S9). Moreover, we observed all indications of cell lysis in these incubations, like the presence of intracellular vesicles and membrane debris.

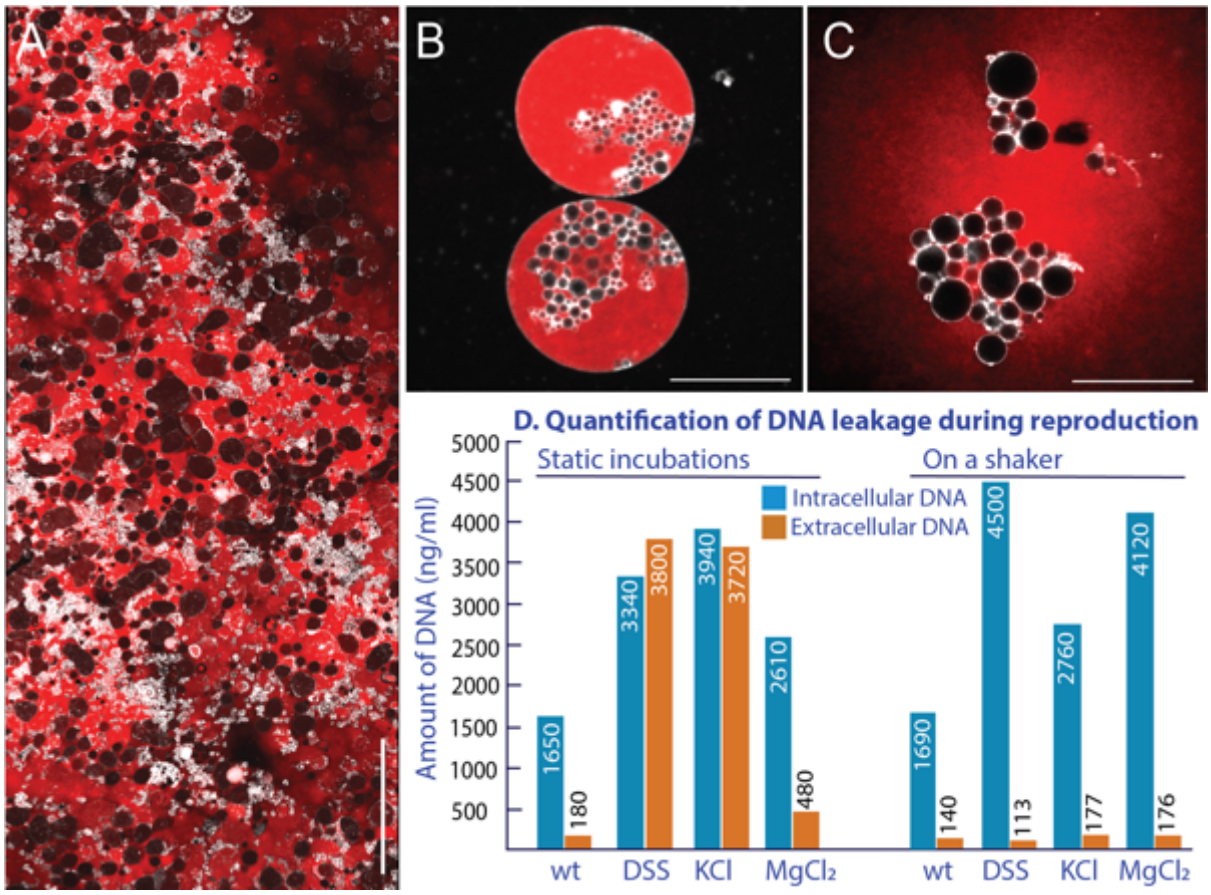

Figure 7. Leakage of cell constituents during *EM-P*'s reproduction. Image A shows *EM-P* cells during the early-log phase. Cells in these images were stained with FM™5-95 (membrane, white) and PicoGreen™ (DNA, red) and imaged using a STED microscope. Image A shows the presence of a considerable amount of extracellular DNA. Image B&C show late log phase cells with intracellular vesicles. They show the same two cells before (B) and after lysis (C). Hollow intracellular vesicles and presence of extracellular DNA (red) can

be seen in image C. Scale bars: 10µm. Image D show the results of the quantification of DNA leakage during *EM-P's* late log growth stage (Figure S10, for all growth stages). wt – wild type (*Exiguobacterium strain M* with a cell wall); DSS, KCl & $MgCl_2$: *EM-P* grown in TSB amended with 6% of the respective salts. Data in D represent mean values of biological repetitions from different batches of *EM-P*'s inoculum's (n=5).

Compared to *EM*, and all *EM-P* incubations exhibited a higher concentration of extracellular DNA, when grown under station conditions (Figure 7 & S8). A similar trend was observed in the intracellular and extracellular DNA ratio when *EM-P* was grown in media containing DSS or KCl (Figure 7 & S8). In comparison, less leakage of DNA was observed when cells were grown in media containing $MgCl_2$ (Figure 7 & S8). We also observed less leakage of DNA when *EM-P* was grown on an orbital shaker compared to static incubations (Figure 7 & S8). No significant differences were observed between the native *EM* and *EM-P* in terms of DNA leakage when *EM-P* cells were grown in media containing $MgCl_2$ on an orbital shaker.

Staining and subsequent quantification by flow cytometry showed that ≅ 80 to 85% of the daughter cells receive DNA from the parent cells and exhibited cytoplasmic enzyme activity (Figures 8, S10 & S11). The viability of daughter cells was also evident from the growth of daughter cells when transferred into a new media.

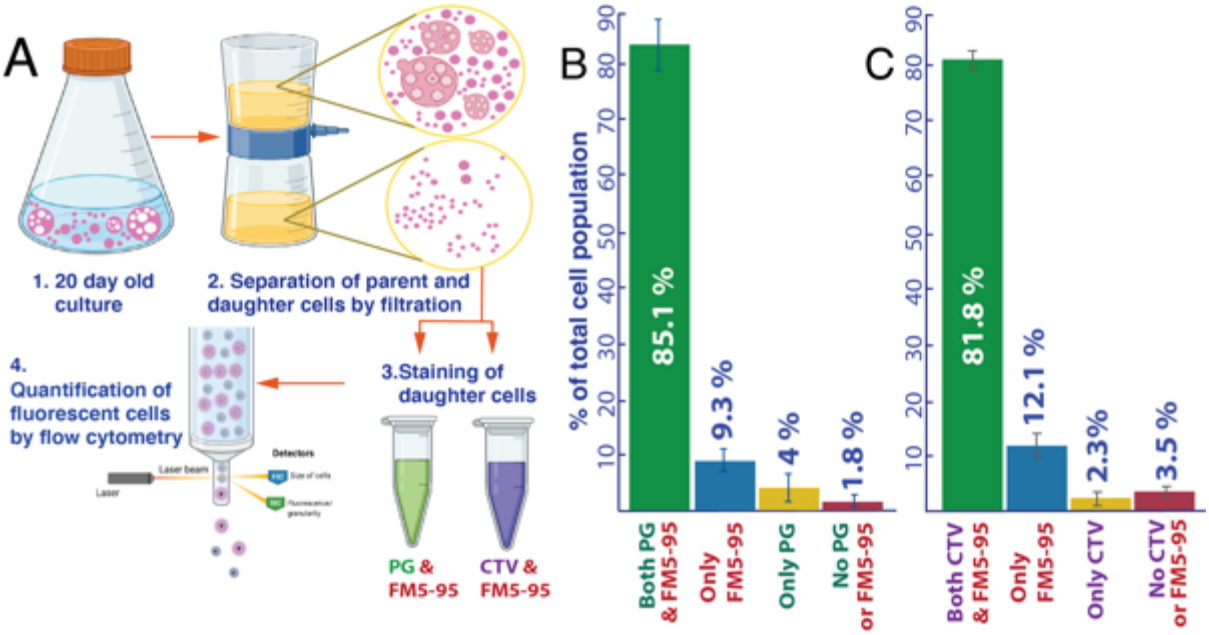

Figure 8. Metabolic viability of daughter cells. Panel A shows the workflow of the experiment. Image B shows the results of this quantification of these cells by flow cytometry. The green bar shows the percentage of cells containing both an intact membrane and intracellular DNA (FM^{TM}5-95 & PG). The subsequent blue, yellow, and red bars show the percentages of cells that were either deficient in intracellular DNA or an intact membrane or both respectively. Image C shows the results of this quantification of different cell population flow cytometry. The green bar shows the percentage of cells containing both an intact membrane and intracellular enzyme activity (FM^{TM}5-95 & CTV). The subsequent blue, yellow and red bars show the percentages of cells that were either deficient in intracellular enzyme activity or an intact membrane or both respectively. The original flow cytometry plots together with the confocal microscope images of daughter cells were shown in Figures S10 & S11.

Discussion

The physiological differences observed between *EM* and *EM-P* could be explained by the loss of coordination between metabolic processes within the protoplasts. Unlike *EM*, *EM-P* exhibited an excessive lipid synthesis (Figure S2), high catalase activity irrespective of the environmental conditions, and inefficient use of oxygen as a terminal electron acceptor even when grown in well-aerated media (Figure S1). Within a normal functioning cell, lipid synthesis is regulated to match the surface area and the growth rate (i.e., rate of cell volume/surface area increase). The excessive synthesis of lipids in *EM-P* is evident from the membrane structures within the cytoplasm (Figure 5 & S2) and the filamentous extensions on the cell surface (Figure 2&3). Some cells were had large lipid globules (Figure S2), also suggesting excessive lipid synthesis in *EM-P*. A similar loss of metabolic coordination leading to excessive lipid synthesis was reported previously in bacterial protoplasts[8]. We speculate that the accumulation of fermentation products while growing in a well-aerated media[21] and an erratic catalase activity[22] could also be related to the discrepancy in lipid synthesis and membrane phase separation.

The membrane lipid composition and fluidity are known to exert a quantitative influence on the outcome of the electron transport system (ETC)[23]. Much of this effect is currently explained by the relation between the fluidity and the diffusion-coupled electron transfer by ubiquinone between the ETC complexes[23]. However, the relation between membrane composition, liquid-liquid phase separation, ETC activity is still poorly understood. The accumulation of fermentation products, when grown in well-aerated media, suggests a reduced efficiency of ETC in protoplasts (Figure S1), *EM-P* was observed to have diverted 20-25% of the total glucose towards fermentation rather than more efficient oxidation to CO_2

by citric acid cycle[21]. However, this reduce efficiency or complete absence ETC function during anaerobic incubations is not evident from *EM-P*'s catalase activity.

Reactive oxygen species (ROS) are known to be produced during the flow of electrons through the ETC[24]. To prevent oxidative damage caused by ROS, cells are known to produce the enzymes catalase and superoxide dismutase [25]. In a normally functioning cell, the expression of such enzymes is inhibited during growth by fermentation due to the absence of ETC activity. Such enzymes are selectively produced during growth by respiration[25]. In accordance with these predictions, *EM* exhibited high and low catalase activity during aerobic and anaerobic growth conditions, respectively. In contrast, *EM-P* showed consistent catalase activity, regardless of its physiology or the presence of terminal electron acceptors. These physiological differences between *EM-P* and *EM* indicate a lack of molecular biological mechanisms for perceiving environmental conditions or a loss of biological coordination necessary to adapt cellular physiology to environmental conditions[26] in *EM-P*. Loss of metabolic coordination leading to chaotic cell behavior, like excessive lipid synthesis[8] and a lack of ability to assemble a peptidoglycan cell wall, despite the upregulation of cell wall synthesis genes[27] and increased ROS activity[28], were previously reported in protoplasts. Even though the behavior of *EM-P* is in tune with earlier studies on protoplasts[8,27,28], more extensive molecular biological investigations are required to further substantiate this claim. We believe such investigations are beyond the scope of understanding the life cycle of such cells under the environmental conditions of early Earth.

Even though the above observations suggest a loss of coordination between intracellular processes, this did not result in an entirely random reproduction. The life cycle and plethora of morphologies exhibited by *EM-P* could be explained by the biophysical properties of *EM-*

P's cell constituents, growth rate, and unorderly molecular biological regulatory processes leading to excessive lipid synthesis[8] and environmental conditions. The excessive lipid synthesis in protoplasts results in a cell state where the membrane surface area far exceeds the surface area of the cell. When a similar state is induced in LVs by applying osmotic stress, vesicles undergo shrinkage in a sequence of steps involving the formation of buds and filamentous extensions[29,30]. The morphological transformation of *EM-P* observed in our study was similar to LVs undergoing osmotic shrinkage[20,31]. Like the LVs, morphologies of *EM-P* within a given growth stage could be explained by the rate of cytoplasmic volume increase (i.e., its growth rate), expansion strain on the membrane surface, and the amount of excess membrane.

The absence of either filamentous extensions or membrane lumps within the log phase cell (Figure 1) suggests that the rate of cytoplasmic volume increases (i.e., its growth rate) during this growth phase kept pace with lipid synthesis. Reproduction of cells in this growth phase visually resembles budding or binary fission, depending on the size of the daughter cells (Figure 1&9). Despite numerous repetitions, no uniformity was observed either in the sizes or number of daughter cells formed from a single *EM-P* cell (Video 1-3). This method of reproduction and lack of uniformity in the sizes of the daughter cells could be explained by the complex composition of the bacterial cell membrane and the relatively rapid growth rate of cells in their log phase.

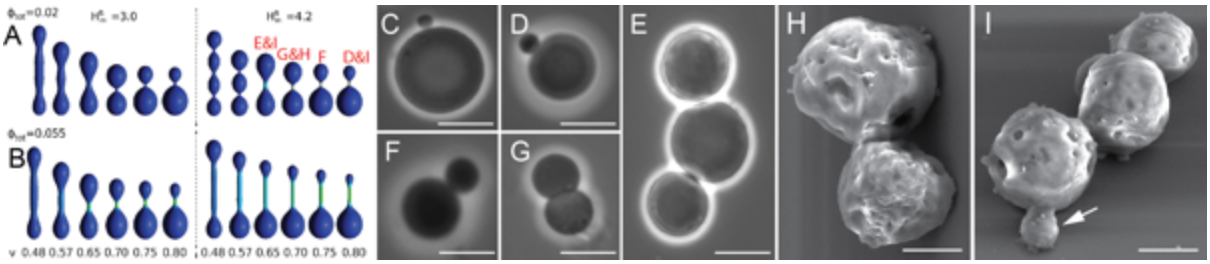

Figure 9. Asymmetric division of *EM-P* during log-phase. Images A & B show theoretically predicted morphologies of vesicles with lateral membrane heterogeneity[32]. ν is the ratio between the actual volume of a vesicle to the volume of a vesicle in its spherical form with the same surface area, Φ_{tot} is the concentration of the membrane component that differed in its intrinsic membrane curvature, H^B_m (originally published by Bobrovska *et al*., 2013)[32]. Images C-I show, phase-contrast (C-E) and SEM (H & I) images of *EM-P* cells undergoing a similar method of reproduction. Similarities between *EM-P* cells and predicted morphologies is indicated in image A (letters in red). Scale bars: 10μm (C-E) & 2μm (H & I).

Most previous attempts at understanding the biophysical properties of protocells were conducted on LVs of simple chemical composition. In such studies, the physical properties of membranes like elasticity and spontaneous curvature along their surface remain largely homogeneous. Unlike LVs, cell membranes are composed of numerous lipids species, quinones, membrane proteins, and in case of *EM-P* a diverse composition of carotenoid pigments[33]. This diverse composition results in the formation of lipid-lipid[34] and lipid-protein[35] nanodomains with different physical properties[32] along the surface of the cell membrane. In theory, such lateral heterogeneity in the physical property's leads could to asymmetric fission of cells (Figure 1). The size and morphology of the daughter cells formed by this process is thought to have been determined by the level of heterogeneity in the cell membrane and by reduced volume (ν), i.e., the difference between the actual volume of the cell (V) and the volume of the cell in its spherical form (V_s). In the case of *EM-P,* the ν-values depend on the amount of excess membrane. The high lateral membrane heterogeneity expected in live cell membranes and the relative lack of excess cell membrane during the log phase (i.e., ν-values could have been closer to 1.0) could explain the reproduction by budding

and binary fission. A comparison of theoretically predicted morphologies of LVs and *EM-P* is shown in Figure 9.

With a gradual reduction of growth rate towards the late log phase, the rate of membrane synthesis seems to have far exceeded the rate of cytoplasmic volume increase. This imbalance between the surface area of the cell and the plasma membrane could have resulted in the formation of hollow membrane extensions (Figure 2), lipid globules (Figure S2) or intracellular vesicles (Figure 3) as a mechanism of accommodating the excess membrane[20]. These observations suggest that growth rate influenced the morphology of *EM-P*. Accordingly, when we kept cells in a prolonged log phase, they did not form external and internal membrane structures. This supports our inference that the balance between lipid synthesis and cytoplasmic growth determines cell morphology. Cells under these conditions consistently reproduced by budding or binary fission, like the ones shown in Figure 1.

The formation of external and inter-membrane structures can also be explained by the model proposed by Lipowsky & Jülicher[36,37]. It was proposed that phase-separated membranes tend to undergo budding to minimize interfacial energy at the phase boundary to attain a thermodynamically stable state. They do so by forming an out-of-plane membrane invagination, which gradually transforms the softer liquid-disordered (L_d) membrane into a bud (Figure 5). Earlier studies hypothesized that the L_d membrane most likely undergoes budding due to its low bending rigidities and high spontaneous curvature[20]. In accordance with this theory[34], budding in *EM-P* is associated with phase separation of the cell membrane (Figure 5). L_d membrane initially appeared as small patches on the cell surface, less than 180nm in diameter (Figure 5A-C). As predicted by the theoretical propositions, as the area of the L_d membrane increased, it underwent budding, possibly due to a gradual increase in the

line tension at the phase-boundary[38] (Figure 5 & Video 19). Nevertheless, some deviations from this expected behavior were observed. The first was the difference in the direction of budding. Contrary to the predictions, we observed L_d-membrane consistently underwent a negative (into the cell) rather than positive (out of the cell) curvature (Figure 5). Second, despite its higher bending rigidity, the liquid-ordered (L_o) membrane also underwent deformation out of the cell (Figure 5G-I, closed arrows & Video 19). Intriguingly, all positive (out of the cell) membrane deformations were exclusively composed of L_o-membrane, and all negative membrane deformations (into the cell) were exclusively composed of L_d-membrane (Figure 5, S6 & Video 19).

The direction and physical nature of a membrane undergoing budding could be explained by its lipid composition[39], and the nature of the aqueous core[40]. Bacia *et al.* studied the influence of membrane sterol composition on budding[39] and reported that nature and direction of budding is influenced by the nature and concentration of sterols in the membrane. Despite higher bending rigidities, this study showed that some sterols could induce preferential budding of more rigid L_o membrane instead of L_d membrane. Prokaryotes lack sterols like cholesterol and its derivatives but possess functional analogs of cholesterol, like hopanoids[41]. The properties of these compounds in inducing membrane phase separation and budding were rarely investigated. Apart from sterols, invagination of a more rigid L_o membrane was also reported to happen when LVs[29] experience a state of excess membrane (like during the osmotic shrinkage), possibly due to an increase in the spontaneous curvature of L_o membrane due to excess lipids[20]. The nature and direction of the membrane invagination could also have been determined by the packing densities of the aqueous core (cytoplasm) and the growth media surrounding the cell[40]. Studies showed when liquid-liquid phase-separation was induced in the aqueous core (not the membrane), the vesicle membrane too, underwent phase

separation according to their densities[20,42]. The denser phase of the aqueous core was observed to have been associated with L_d membrane and the lighter phase with L_o membrane[40]. This could explain the invagination of the L_d membrane into the cell, given the higher densities of cytoplasm (~17-35 wt% molecules). Preference of the L_o membrane to the comparatively less dense growth media (~6-7 wt% molecules) could have led to the L_o membrane undergoing positive curvature, i.e., out of the cell (Figure 5 & Video 20). TEM images of cells shown in Figure 4, show these differences in the packing densities between the cytoplasm and surroundings[43].

The sequence of steps involved in the formation of filamentous extensions (Figure 2) is in accordance with our inference that morphology of *EM-P* is dependent on the growth rate of the cell. LVs undergoing osmotic shrinkage were known to develop filamentous extensions. The formation of such filamentous extensions in LVs depends on the osmolarity of the media and rate of osmotic shrinkage[20]. Slow transfer of lipid from the parent cell into these filamentous extensions[20] led to the formation of shorter membrane extensions from multiple sites on the cell surface. A relatively faster rate of lipid transfer, led to the extension of already formed filaments rather than forming of new filaments. In case of *EM-P,* we argue that rate of lipid transfer is dependent on its growth kinetics. During the log phase when the growth rate is high, cytoplasmic volume increase kept pace with the membrane synthesis i.e., less membrane was available for formation of hollow filamentous extensions. Hence during this growth stage, formation of small surface invaginations at multiple sites is favored (Figure 2). During the later growth-stage, the ratio of cytoplasmic volume increase to amount of excess membrane is low i.e., more membrane area is available for the formation of hollow filamentous extensions. Under such conditions, it is energetically favorable for existing filaments to increase in length (Figure 2E&F), rather than forming new ones.

The transformation of hollow extracellular and intravesicular filamentous extensions into a string-of-spherical daughter cells could be explained by two different mechanisms. One could have been the spontaneous transformation of tubular vesicles into a string-of-beads morphology to reduce the interfacial area to reach a thermodynamically stable lower energy state[42] (Video 22). A similar transformation of filamentous structures was reported previously LVs, especially the one undergoing osmotic shrinkage[42,44]. This inherent tendency of tubular vesicles to spontaneously deform into a "string-of-beads" morphology could have led to the formation of spherical daughter cells (Figures 2&3). Alternately, the formation of daughter cells could also be explained simply by the lower volume of cytoplasm that was transferred into the filaments compared to the total volume of the filament[20]. The excess membrane within these tubular structures should have collapsed and transformed into tethers connecting adjacent daughter cells (Figures 2&3).

The random or explosive lysis of bacterial cells the leakage of intracellular DNA was not previously reported. However, similar rupture of LVs by two different mechanisms is previously known. This lysis of LVs was explained either due to osmotic pressure created by ROS[45] or by interactions between DNA and lipid head groups[46]. Given no quantitative differences were observed when cells were incubated under anoxic conditions in the dark and imaged using phase-contrast microscopy, we do not presume that this was an imaging artifact caused by confocal laser induced ROS production[47]. Hence, we presume that lysis of cell (Figures 7&S12) could have been mediated by processes other than ROS production and possibly due to the interactions between the nucleic acids and cell membrane[46].

One key aspect of the cell cycle is the fission of the parent cell into metabolically viable daughter cells. Multiple studies have focused on achieving cell division independent of cell-replication machinery. Previous studies achieved fission by mechanical means[48], by encapsulation of protein involved in cell division into LVs[49] or by constantly incorporating new lipids into the LVs[2]. Given that *EM-P* was grown under static conditions, we do not presume that the cell division was a result of an external forces. Recent studies suggest proteins involved in canonical cell-replication process could result in cell surface undulations, destabilizing and ultimately resulting in division of vesicles[49]. We observed *EM-P* in a similar state of surface undulations. We propose that this intrinsically unstable nature of *EM-P* could have resulted in a spontaneous cell division (Video 1-3) and the fragmentation of string-of-daughter cells (Video 8-10). Nonetheless, we do not presume fission in *EM-P* was caused by a specific protein, as treatment of cells with bactericidal chemicals like sodium azide (0.3%)[50] or protein polymerizing agents like 0.5% glutaraldehyde and formaldehyde[51] did not result in a static cell. These surface undulations or movement of cells could only be halted by osmotically equilibrating cytoplasm with the surrounding (by treating cells with Triton X100). This suggests that these surface deformations were caused either by the differences in osmolarities between the cytoplasm and the surrounding media[52] or due to the Brownian movement of intracellular constituents[53] (Video 23, movement of DNA within the cell). A similar case of cell division due to the Brownian movement of intracellular constituents was shown by earlier studies both in droplets[54] and LVs[49,53]. These observations suggest that cell division in *EM-P* was a result of the biophysical properties of cell constituents rather than the molecular biological processes within the cell.

The biophysical properties of cell constituents are determined by environmental conditions. For instance, different cations interact differently with the cell membrane and alter their

physical properties[31,55,56]. To understand how *EM-P*-like cells could have reproduced under a wide range of environmental conditions, we tested the influence of individual salts and external physical forces on its reproduction. Considerable differences were observed in the morphology and reproduction of *EM-P* under different environmental conditions. Differences in the cell sizes, when grown in the presence of monovalent and divalent salts, can be explained by the nature of interactions between cations and phospholipid head groups[31]. Interaction of monovalent cations like potassium was known to increase the membrane's fluidity, whereas divalent cations like magnesium decrease the fluidity[55]. This increase in membrane fluidity could have facilitated the expansion of cells in incubations containing DSS and KCl[31], resulting in relatively larger cells. Increased membrane rigidity when grown in the presence of $MgCl_2$ accordingly led to the formation of smaller cells (Figure 6). The reasons for the reproduction predominantly via extracellular daughter in the presence of $MgCl_2$ and predominantly via intracellular daughter cells in the presence of KCl are currently unclear. Nevertheless, a similar phenomenon of intracellular vesicle formation in the presence of KCl was observed previously in LVs[31]. Apart from the visible differences in morphologies, *EM-P* reproduced more efficiently when grown in the presence of $MgCl_2$, compared to DSS or KCl (Figures 7 & S8). This improved efficiency could be attributed to reproduction by the formation of external daughter cells in $MgCl_2$, which could have eliminated the need for cell lysis to release the intracellular daughter cells. *EM-P* reversibly changes its morphology when transferred between media of different salt compositions. This suggests that the chemical composition of the growth media (i.e., environmental conditions), rather than the information encoded in its genome, influenced the morphology of *EM-P*.

Unlike the growth conditions used in our experiments, cells within the natural environments are rarely static. Archaean Eon Earth is thought to have a greater intensity of waves than the

present-day Earth due to the closer proximity of the moon[57]. Protocells inhabiting early Earth's oceans or shorelines would have been subjected to constant agitation due to this wave action. To understand the influence of such physical forces on *EM-P*'s morphology and reproductive processes, we grew *EM-P* on an orbital shaker. Growth under non-static conditions had a significant effect on both the method and the reproduction efficiency (Figures 7 & S8). In the presence of divalent cations, the reproductive efficiency of *EM-P* was similar to cells in their native state, suggesting that protocells could have reproduced rather efficiently under environmental conditions of early Earth, despite the lack of dedicated molecular biological processes.

The method of reproduction we described here closely resembles the reproductive process of minimal cells that were a result of a top-down synthetic biology approach[58] (Figures S13 - S15) as well as mathematical simulations of the protocell reproduction process[59] (Figure S16 & S17). Like *EM-P*, both these approaches resulted in cells that reproduce either by asymmetric cell division (Figure S16) or by forming a string of daughter cells (Figure S14&S15) and exhibit the formation of hollow intracellular vesicles (Figure S14). Nevertheless, our proposal that protocells reproduced by this process is predicated on three fundamental presumptions. First, Earth's oceans should have a salt content of 5-10% w/v, similar to the growth conditions employed in our study. These conditions are required to maintain a state of osmotic non-equilibrium between the cell and its surrounding[31,52], which is necessary to keep cells in a constant state of surface oscillation. In our opinion, such surface undulations could have played an essential role in mediating cell division (Video 1-10). Second, the membranes of these protocells should have been of complex phospholipid composition. An osmotic non-equilibrium with the surrounding can only be maintained for a prolonged period if the membrane is composed of phospholipids rather than considerably

more permeable fatty acid[4]. Cell membranes of complex phospholipid composition are also necessary to resist precipitation or crystallization of phospholipids and to establish a lateral heterogenicity[60,61], which is required for budding and the ultimate formation of daughter cells. Third, given the impermeability of phospholipid membranes to polar compounds, by the time the above-described processes became prevalent, protocells already should have evolved metabolic pathways for energy conservation and biochemical processes for the synthesis of cell constituents[4], rather than passively taking up pre-synthesized organic carbon from the surroundings. For these reasons, we believe that protocells reproducing by the above-described processes represent an evolutionarily more advanced (*i.e.,* late) state of protocells. Inferences from early Earth's geological, paleontological, and environmental studies agree with all three prerequisites.

A geological argument for the higher salinities of early Earth oceans and paleontological evidence supporting this hypothesis, at least for the Archaean Eon oceans, was presented in the introduction section of this manuscript. Although in theory, environmental conditions of early Earth seem to be conducive for the above-described processes to happen[19], arguing that protocells possessed an internal metabolism and that their membranes were composed of diverse phospholipids first requires us to provide empirical evidence for the existence of such cells on early Earth. Unlike other theories on evolution, the existence of protocells has not been proven empirically.

One important observation of our study was the influence exerted by environmental conditions on primitive cell morphologies. Given the cell in our study are grown under the environmental conditions of early Earth, and in all likelihood, primitive cells lacked complex intracellular processes, we looked into the paleontological record of early Earth (between

3800-2500 million years old) for the possible existence of cells that resemble the ones from our study. Extensive morphological comparison of microfossils with cells from our study showed beyond a reasonable doubt that cells reproducing by the processes we described here existed on early Earth[62]. Microfossil elemental and isotopic signature suggests that these fossilized cells were metabolically active[14,63]. Moreover, spatial differences in the carbon isotope composition in these fossilized cells indicated that their cell membranes exhibited lateral heterogeneity[64,62], similar to *EM-P* cells. An extensive morphological comparison of the microfossils with *EM-P* cells will be presented in a subsequent manuscript. Given these similarities between the results of our study, Archaean Eon microfossils, top-down[58], and bottom-up approaches to understanding early life, we propose with a greater confidence that protocells reproduced by a process similar to that of *EM-P*.

In conclusion, our results suggest that reproduction is an intrinsic biophysical property of cells with an internal metabolism. Reproduction can happen spontaneously, without a need for a dedicated molecular biological process. Given the remarkable similarities between the *EM-P*'s method of reproduction and earlier studies on LVs, we propose mechanistic similarities between these two processes. Given the efficiency with which these cells reproduced under the environmental conditions of early Earth, we presume unilamellar, or the Gram-positive protocells could have reproduced by this process. Our subsequent geological/palaeontological studies further substantiate this claim. To the best of our knowledge, ours is the only study to provide direct evidence of the existence of LVs-like cells or protocells on early Earth.

Video description

Video 1: log phase *EM-P* cells. Cells in these incubations were never static and exhibited continuous surface undulations. Scale bar: 5µm.

Video 2: Log phase *EM-P* cell. Cells with-in different stages of binary fission can be seen in this movie – ovoid cells and cells that were segregated into two daughter cells. Like the cells in video 1, most cells in this growth stage showed surface undulations. Scale bar: 5µm.

Video 3: *EM-P* cells undergoing binary fission but still connected by narrow membrane tethers. Scale bar: 5µm.

Video 4 & 5: These videos show sequential stages involved in the formation of external filamentous extensions. Video 4 shows late log phase *EM-P* cell with filamentous and hollow spherical extensions. Video 5 show gradual increase in the number of such filamentous extensions Scale bar: 5µm.

Videos 6 to 8: These videos show sequential stages involved in the formation of external daughter cells. Videos 6 to 8 show a gradual increase in the length of filamentous extensions and formation of daughter cells. Scale bar: 5µm.

Video 9 & 10: These movies show constant movement of individual daughter cells within the filaments. This push and pull motion of cells within a string could have led to the rupture of membrane tethers (Video 9) connecting daughter cells, leading to the formation of individual daughter cells. Scale bar: 5µm.

Video 12: *EM-L* cell with an intracellular vesicle. Like the external filamentous extensions, intracellular vesicles too were in a constant movement. Scale bar in movie is 5µm.

Video 13: *EM-P* cell with an intracellular vesicle. Cells in these images were stained with FM™5-95 (membrane, cyan) and PicoGreen™ (DNA, red). Bud-like structures originating from different regions of the intracellular vesicles can be seen within the cells. Scale bar: 10μm.

Video 14: Movie shows an *EM-P* cell with an intracellular vesicle containing both individual daughter cells and a string of daughter cells. Scale bar:10μm.

Videos 15-16: *EM-P* cell undergoing lysis and releasing intracellular vesicles. Scale bar:5μm.

Videos 17: Late growth stage *EM-P* cells or intracellular vesicles that were release by the lysis of *EM-P* cells with highly motile internal daughter cells. Scale bar: 5μm.

Video 18: Slow motion movie of *EM-P* vesicles undergoing membrane rupture and releasing of daughter cells. Scale bar: 5μm.

Video 19: *EM-P* cells stained with FM™5-95 (all membrane, red) and FAST DiI™ (L_d-membrane, green). Most L_d (green) membrane is localized to regions within the cells whereas the membrane extending out of the cell is largely devoid of L_d-membrane. Scale bar: 5μm.

Video 20 & 21: *EM-P* cells grown in 5%$MgCl_2$. Video 21 is the magnified region of video 20, showing the constant movement of daughter cells within the filaments. Scale bar: 5μm.

Video 22: *EM-P* with multiple hollow filamentous extensions. Cells in these images were stained with FM™5-95 (membrane, cyan) and PicoGreen™ (DNA, red). A constant change in the morphology of filamentous from tubular to string-of-beads can be seen in the video. Scale bar: 5µm.

Video 23: Early growth stage *EM-P* cells. Cells in these images were stained with FM™5-95 (membrane, cyan) and PicoGreen™ (DNA, green). In most cell's DNA is in a constant state of movement. Scale bar: 5µm.

Video 24: Movie shows mid growth stage *EM-P* cells, undergoing lysis and release of DNA. Cells in these images were stained with FM™5-95 (membrane, red) and PicoGreen™ (DNA, green). Scale bar: 5µm.

Video 25: Movie shows late log phase *EM-P* cells, undergoing lysis. Scale bar: 5µm.

Acknowledgments

We want to thank Petra Schwille for her support and scientific input throughout the work and in preparing the manuscript. Gabriella Berthal, and Markus Oster for excellent technical support. We thank the Advanced Light Microscopy Facility at EMBL, Heidelberg, Ulf Schwartz from Leica Microsystems, and colleagues at the departments of Ecological Microbiology (Bayreuth University) and of Cellular and Molecular Biophysics (Max Planck Institute for Biochemistry) for their support throughout the work.

Author contributions

Conceptualization: DK, ML, BZ & TL. Culture experiments: DK. Electron microscopy: DK & AK. Light microscopy: DK & ML. Analysis: DK & JHK. Manuscript Writing: DK & JHK.

Funding

This research was funded by the European Research Council (ERC) grant agreement 616644 (POLLOX), and by the Deutsche Forschungsgemeinschaft (DFG) grant agreements DFG-TRR174 and Seed funding from Excellence Cluster ORIGINS EXC2094 – 390783311.

Conflicts of Interest

The authors declare that there are no conflicts of interest regarding the publication of this article.

Data Availability

All data, materials, and methods will be shared by Dr. Dheeraj Kanaparthi upon reasonable request.

References

1. Oparin, A.I. (1969). Chemistry and the origin of life. R. Inst. Chem. Rev. 10.1039/rr9690200001.

2. Zhu, T.F., and Szostak, J.W. (2009). Coupled growth and division of model protocell membranes. J. Am. Chem. Soc. *131*, 5705.

3. Hanczyc, M.M., Fujikawa, S.M., and Szostak, J.W. (2003). Experimental models of primitive cellular compartments: encapsulation, growth, and division. Science *302*, 618–622.

4. Budin, I., and Szostak, J.W. (2011). Physical effects underlying the transition from primitive to modern cell membranes. Proc. Natl. Acad. Sci. *108*, 5249–5254.

5. van Heijenoort, J. (2007). Lipid Intermediates in the Biosynthesis of Bacterial Peptidoglycan. Microbiol. Mol. Biol. Rev. *71*. 10.1128/mmbr.00016-07.

6. Bouhss, A., Trunkfield, A.E., Bugg, T.D.H., and Mengin-Lecreulx, D. (2008). The biosynthesis of peptidoglycan lipid-linked intermediates. FEMS Microbiol. Rev. *32*. 10.1111/j.1574-6976.2007.00089.x.

7. Leaver, M., Dominguez-Cuevas, P., Coxhead, J.M., Daniel, R.A., and Errington, J. (2009). Life without a wall or division machine in Bacillus subtilis. Nature *457*, 849.

8. Mercier, R., Kawai, Y., and Errington, J. (2013). Excess membrane synthesis drives a primitive mode of cell proliferation. Cell *152*, 997–1007.

9. Errington, J. (2013). L-form bacteria, cell walls and the origins of life. Open Biol. 10.1098/rsob.120143.

10. Wu, L.J., Lee, S., Park, S., Eland, L.E., Wipat, A., Holden, S., and Errington, J. (2020). Geometric principles underlying the proliferation of a model cell system. Nat. Commun. *11*. 10.1038/s41467-020-17988-7.

11. Monnard, P.-A., Apel, C.L., Kanavarioti, A., and Deamer, D.W. (2002). Influence of ionic inorganic solutes on self-assembly and polymerization processes related to early forms of life: Implications for a prebiotic aqueous medium. Astrobiology *2*, 139–152.

12. Mojzsis, S.J., Harrison, T.M., and Pidgeon, R.T. (2001). Oxygen-isotope evidence from ancient zircons for liquid water at the Earth's surface 4,300 Myr ago. Nature *409*. 10.1038/35051557.

13. Mojzsis, S.J., Arrhenius, G., McKeegan, K.D., Harrison, T.M., Nutman, A.P., and Friend, C.R.L. (1996). Evidence for life on Earth before 3,800 million years ago. Nature *384*. 10.1038/384055a0.

14. Dodd, M.S., Papineau, D., Grenne, T., Slack, J.F., Rittner, M., Pirajno, F., O'Neil, J., and Little, C.T.S. (2017). Evidence for early life in Earth's oldest hydrothermal vent precipitates. Nature *543*, 60–64.

15. Schopf, J.W. (1993). Microfossils of the Early Archean Apex chert: new evidence of the antiquity of life. Science *260*, 640–646.

16. Põldsalu, I., Koksal, E.S., Friis, H., Mojzsis, S., Bizzarro, M., and Gozen, I. (2022). Spontaneous formation of prebiotic compartment colonies on Hadean Earth and Pre-Noachian Mars. Biophys. J. *121*. 10.1016/j.bpj.2021.11.2351.

17. Blake, R.E., Chang, S.J., and Lepland, A. (2010). Phosphate oxygen isotopic evidence for a temperate and biologically active Archaean ocean. Nature *464*. 10.1038/nature08952.

18. Catling, D.C., and Zahnle, K.J. (2020). The Archean atmosphere. Sci. Adv. *6*. 10.1126/sciadv.aax1420.

19. Knauth, L.P. (1998). Salinity history of the Earth's early ocean. Nature *395*, 554.

20. Liu, Y., Agudo-Canalejo, J., Grafmüller, A., Dimova, R., and Lipowsky, R. (2016). Patterns of flexible nanotubes formed by liquid-ordered and liquid-disordered membranes. ACS Nano. 10.1021/acsnano.5b05377.

21. Luengo, A., Li, Z., Gui, D.Y., Sullivan, L.B., Zagorulya, M., Do, B.T., Ferreira, R., Naamati, A., Ali, A., Lewis, C.A., et al. (2021). Increased demand for NAD+ relative to ATP drives aerobic glycolysis. Mol. Cell *81*. 10.1016/j.molcel.2020.12.012.

22. Saito, Y., and Kimura, W. (2021). Roles of Phase Separation for Cellular Redox Maintenance. Front. Genet. *12*. 10.3389/fgene.2021.691946.

23. Budin, I., Rond, T. de, Chen, Y., Chan, L.J.G., Petzold, C.J., and Keasling, J.D. (2018). Viscous control of cellular respiration by membrane lipid composition. Science *362*. 10.1126/science.aat7925.

24. Zorov, D.B., Juhaszova, M., and Sollott, S.J. (2014). Mitochondrial reactive oxygen species (ROS) and ROS-induced ROS release. Physiol. Rev. *94*. 10.1152/physrev.00026.2013.

25. Hertel, C., Schmidt, G., Fischer, M., Oellers, K., and Hammes, W.P. (1998). Oxygen-dependent regulation of the expression of the catalase gene katA of Lactobacillus sakei LTH677. Appl. Environ. Microbiol. *64*. 10.1128/aem.64.4.1359-1365.1998.

26. Ryall, B., Eydallin, G., and Ferenci, T. (2012). Culture History and Population Heterogeneity as Determinants of Bacterial Adaptation: the Adaptomics of a Single Environmental Transition. Microbiol. Mol. Biol. Rev. *76*. 10.1128/mmbr.05028-11.

27. Studer, P., Borisova, M., Schneider, A., Ayala, J.A., Mayer, C., Schuppler, M., Loessner, M.J., and Briers, Y. (2016). The Absence of a Mature Cell Wall Sacculus in Stable Listeria monocytogenes L-Form Cells Is Independent of Peptidoglycan Synthesis. PLoS ONE *11*. 10.1371/journal.pone.0154925.

28. Kawai, Y., Mercier, R., Wu, L.J., Domínguez-Cuevas, P., Oshima, T., and Errington, J. (2015). Cell growth of wall-free L-form bacteria is limited by oxidative damage. Curr. Biol. *25*, 1613–1618.

29. Yanagisawa, M., Imai, M., and Taniguchi, T. (2008). Shape deformation of ternary vesicles coupled with phase separation. Phys. Rev. Lett. 10.1103/PhysRevLett.100.148102.

30. Yanagisawa, M., Imai, M., and Taniguchi, T. (2010). Periodic modulation of tubular vesicles induced by phase separation. Phys. Rev. E - Stat. Nonlinear Soft Matter Phys. 10.1103/PhysRevE.82.051928.

31. Karimi, M., Steinkühler, J., Roy, D., Dasgupta, R., Lipowsky, R., and Dimova, R. (2018). Asymmetric Ionic Conditions Generate Large Membrane Curvatures. Nano Lett. 10.1021/acs.nanolett.8b03584.

32. Bobrovska, N., Góźdź, W., Kralj-Iglič, V., and Iglič, A. (2013). On the Role of Anisotropy of Membrane Components in Formation and Stabilization of Tubular Structures in Multicomponent Membranes. PLoS ONE. 10.1371/journal.pone.0073941.

33. Jinendiran, S., Dahms, H.U., Dileep Kumar, B.S., Kumar Ponnusamy, V., and Sivakumar, N. (2020). Diapolycopenedioic-acid-diglucosyl ester and keto-myxocoxanthin glucoside ester: Novel carotenoids derived from Exiguobacterium acetylicum S01 and evaluation of their anticancer and anti-inflammatory activities. Bioorganic Chem. *103*. 10.1016/j.bioorg.2020.104149.

34. Simons, K., and Ikonen, E. (1997). Functional rafts in cell membranes. Nature. 10.1038/42408.

35. Corradi, V., Sejdiu, B.I., Mesa-Galloso, H., Abdizadeh, H., Noskov, S.Y., Marrink, S.J., and Tieleman, D.P. (2019). Emerging Diversity in Lipid-Protein Interactions. Chem. Rev. *119*. 10.1021/acs.chemrev.8b00451.

36. Lipowsky, R. (1992). Budding of membranes induced by intramembrane domains. J. Phys. II. 10.1051/jp2:1992238.

37. Jülicher, F., and Lipowsky, R. (1993). Domain-induced budding of vesicles. Phys. Rev. Lett. 10.1103/PhysRevLett.70.2964.

38. Baumgart, T., Hess, S.T., and Webb, W.W. (2003). Imaging coexisting fluid domains in biomembrane models coupling curvature and line tension. Nature. 10.1038/nature02013.

39. Bacia, K., Schwille, P., and Kurzchalia, T. (2005). Sterol structure determines the separation of phases and the curvature of the liquid-ordered phase in model membranes. Proc. Natl. Acad. Sci. U. S. A. 10.1073/pnas.0408215102.

40. Andes-Koback, M., and Keating, C.D. (2011). Complete budding and asymmetric division of primitive model cells to produce daughter vesicles with different interior and membrane compositions. J. Am. Chem. Soc. *133*. 10.1021/ja202406v.

41. Sáenz, J.P., Grosser, D., Bradley, A.S., Lagny, T.J., Lavrynenko, O., Broda, M., and Simons, K. (2015). Hopanoids as functional analogues of cholesterol in bacterial membranes. Proc. Natl. Acad. Sci. U. S. A. 10.1073/pnas.1515607112.

42. Li, Y., Lipowsky, R., and Dimova, R. (2011). Membrane nanotubes induced by aqueous phase separation and stabilized by spontaneous curvature. Proc. Natl. Acad. Sci. U. S. A. 10.1073/pnas.1015892108.

43. Sandoz, P.A., Tremblay, C., Gisou van der Goot, F., and Frechin, M. (2019). Image-based analysis of living mammalian cells using label-free 3D refractive index maps reveals new organelle dynamics and dry mass flux. PLoS Biol. *17*. 10.1371/journal.pbio.3000553.

44. Sanborn, J., Oglęcka, K., Kraut, R.S., and Parikh, A.N. (2012). Transient pearling and vesiculation of membrane tubes under osmotic gradients. Faraday Discuss. 10.1039/c2fd20116j.

45. Zhu, T.F., and Szostak, J.W. (2011). Exploding vesicles. J. Syst. Chem. 10.1186/1759-2208-2-4.

46. Angelova, M.I., Hristova, N., and Tsoneva, I. (1999). DNA-induced endocytosis upon local microinjection to giant unilamellar cationic vesicles. Eur. Biophys. J. *28*, 142–150.

47. Artifacts of light (2013). Nat. Methods *10*, 1135–1135. 10.1038/nmeth.2760.

48. Deshpande, S., Spoelstra, W.K., Van Doorn, M., Kerssemakers, J., and Dekker, C. (2018). Mechanical Division of Cell-Sized Liposomes. ACS Nano *12*. 10.1021/acsnano.7b08411.

49. Litschel, T., Ramm, B., Maas, R., Heymann, M., and Schwille, P. (2018). Beating Vesicles: Encapsulated Protein Oscillations Cause Dynamic Membrane Deformations. Angew. Chem. - Int. Ed. 10.1002/anie.201808750.

50. Levy, S., and Chevion, M. (2009). Synergistic cytotoxic effect of tetrachlorocatechol and sodium azide in Escherichia coli: Toxicity, metabolism, and mechanistic aspects. Environ. Toxicol. Chem. *28*. 10.1897/08-518.1.

51. Spahn, C., Grimm, J.B., Lavis, L.D., Lampe, M., and Heilemann, M. (2019). Whole-Cell, 3D, and Multicolor STED Imaging with Exchangeable Fluorophores. Nano Lett. *19*. 10.1021/acs.nanolett.8b04385.

52. Oglęcka, K., Rangamani, P., Liedberg, B., Kraut, R.S., and Parikh, A.N. (2014). Oscillatory phase separation in giant lipid vesicles induced by transmembrane osmotic differentials. eLife. 10.7554/elife.03695.

53. Vutukuri, H.R., Hoore, M., Abaurrea-Velasco, C., van Buren, L., Dutto, A., Auth, T., Fedosov, D.A., Gompper, G., and Vermant, J. (2020). Active particles induce large shape deformations in giant lipid vesicles. Nature *586*. 10.1038/s41586-020-2730-x.

54. Zwicker, D., Seyboldt, R., Weber, C.A., Hyman, A.A., and Jülicher, F. (2017). Growth and division of active droplets provides a model for protocells. Nat. Phys. 10.1038/nphys3984.

55. Tsai, H.H.G., Lai, W.X., Lin, H. Da, Lee, J. Bin, Juang, W.F., and Tseng, W.H. (2012). Molecular dynamics simulation of cation-phospholipid clustering in phospholipid bilayers: Possible role in stalk formation during membrane fusion. Biochim. Biophys. Acta - Biomembr. *1818*. 10.1016/j.bbamem.2012.05.029.

56. Blöchliger, E., Blocher, M., Walde, P., and Luisi, P.L. (1998). Matrix effect in the size distribution of fatty acid vesicles. J. Phys. Chem. B *102*, 10383–10390.

57. Crawford, E.B., Arbic, B.K., Sheldon, N.D., Ansong, J.K., and Timko, P.G. (2022). Investigating the behavior of mid-Archean tides and potential implications for biogeochemical cycling. Precambrian Res. *380*, 106799. 10.1016/j.precamres.2022.106799.

58. Hutchison, C.A., Chuang, R.Y., Noskov, V.N., Assad-Garcia, N., Deerinck, T.J., Ellisman, M.H., Gill, J., Kannan, K., Karas, B.J., Ma, L., et al. (2016). Design and synthesis of a minimal bacterial genome. Science. 10.1126/science.aad6253.

59. Ruiz-Herrero, T., Fai, T.G., and Mahadevan, L. (2019). Dynamics of growth and form in prebiotic vesicles. ArXiv Prepr. ArXiv190104406.

60. Jordan, S.F., Nee, E., and Lane, N. (2019). Isoprenoids enhance the stability of fatty acid membranes at the emergence of life potentially leading to an early lipid divide. Interface Focus. 10.1098/rsfs.2019.0067.

61. Jordan, S.F., Rammu, H., Zheludev, I.N., Hartley, A.M., Maréchal, A., and Lane, N. (2019). Promotion of protocell self-assembly from mixed amphiphiles at the origin of life. Nat. Ecol. Evol. 10.1038/s41559-019-1015-y.

62. Kanaparthi, D., Lampe, M., Zhu, B., Boesen, T., Klingl, A., Schwille, P., and Lueders, T. (2021). On the nature of the earliest known lifeforms. bioRxiv, 2021.08.16.456462. 10.1101/2021.08.16.456462.

63. Wacey, D., Kilburn, M.R., Saunders, M., Cliff, J., and Brasier, M.D. (2011). Microfossils of sulphur-metabolizing cells in 3.4-billion-year-old rocks of Western Australia. Nat. Geosci. *4*, 698–702.

64. Lepot, K., Williford, K.H., Ushikubo, T., Sugitani, K., Mimura, K., Spicuzza, M.J., and Valley, J.W. (2013). Texture-specific isotopic compositions in 3.4 Gyr old organic matter support selective preservation in cell-like structures. Geochim. Cosmochim. Acta *112*, 66–86.